

# Uncertainty on determining the dark energy equation of state due to the spatial curvature

Zhuo-Yi Huang, Bin Wang\*

*Department of Physics, Fudan University,  
Shanghai 200433, People's Republic of China*

Ru-Keng Su<sup>†</sup>

*China Center of Advanced Science and Technology (World Laboratory),  
P.B.Box 8730, Beijing 100080, People's Republic of China*

*Department of Physics, Fudan University,  
Shanghai 200433, People's Republic of China*

## Abstract

We have studied the uncertainty on the determination of the dark energy equation of state due to a non-vanishing spatial curvature by considering some fundamental observables. We discussed the sensitivity of these observables to the value and redshift history of the equation of state and the spatial curvature and investigated whether these different observables are complementary and can help to reduce the cosmic confusion.

PACS numbers: 04.62 +v, 98.80.Cq

---

\*Electronic address: wangb@fudan.edu.cn

<sup>†</sup>Electronic address: rksu@fudan.ac.cn

There is growing observational evidence indicating that our universe is undergoing an accelerated expansion driven by a yet unknown dark energy (DE) [1]. In the past years much effort has been made to understand the nature and the origin of the DE. The leading interpretation of such a DE is a cosmological constant with equation of state (EoS)  $w_D = -1$ . There are other conjectures relating the DE to a scalar field called Quintessence with  $w_D > -1$ , or to an exotic field called Phantom with  $w_D < -1$  [2]. Recently, extensive analysis found that the current data favors DE models with EoS in the vicinity of  $w_D = -1$  [3], straddling the cosmological constant boundary. Since the EoS can give insight into the microscopic nature of DE, it is of particular interest to investigate whether the observations will allow us to determine formally if DE is of the Phantom type, Quintessence type or cosmological constant.

In observations, nearly all proposed tests for the nature of DE measure some combination of four fundamental observables: the Hubble parameter  $H(z)$ , the distance-redshift relation  $d_L(z)$ , the age-redshift relation  $t(z)$ , or the linear growth factor  $D_1(z)$  [4, 5]. Values of these observables are sensitive to redshift and the EoS. Studying DE tests in terms of these observables gives us advantage to see whether and how different observational strategies complement each other so that can help to constrain the DE EoS. In [5], sensitivities of measurements of different observables or of the same observable at different redshifts for constant EoS or dynamic EoS have been discussed and whether these different observables are complementary has been emphasized. Their work was done based on the assumption that the universe is flat and has not included the spatial curvature influence.

Usually, investigations of DE assume a spatially flat universe. However tendency of preferring a closed universe appeared in a suite of CMB experiments [6]. The improved precision from WMAP provides further confidence, showing that a closed universe with positively curved space is marginally preferred [7]. In addition to CMB, recently the spatial geometry of the universe was probed by supernova measurements of the cubic correction to the luminosity distance [8], where a closed universe is also marginally favored. Looking towards future precision of observational data, it is worthwhile examining DE in some detail for a non-flat space. Some attempts at the investigation of DE in the universe with spatial curvature have been carried out [9, 10, 11]. In [9, 10], it was found that a non-flat  $\Lambda$  universe is compatible with the SN+CMB data. The extension of quantifying the parameter space  $(w, \Omega_k^0)$  for the static DE with constant EoS was done in [11]. It was shown from the measurement of the luminosity distance that there is significant uncertainty on the determination of DE EoS due to a non-vanishing spatial curvature. It was argued that this kind of cosmic confusion could be reduced by comparing the luminosity distance measurements at

different redshifts.

The motivation of the present paper is to extend the study of the cosmic confusion caused by the non-vanishing spatial curvature by considering the DE with dynamic EoS. We will choose two time-dependent DE models with different parameterizations:

$$w_D^{\text{I}}(z) = w_0 + w_1 \frac{z}{1+z}, \quad (1)$$

$$w_D^{\text{II}}(z) = w_0 + w_1 \frac{z}{(1+z)^2}. \quad (2)$$

These two models have been extensively discussed in various papers, for example, see [12, 13, 14, 15, 16]. Besides concentrating on the measurements of the luminosity distances as done in [11], we will also examine other fundamental observables, such as the Hubble parameter  $H(z)$ , the linear growth factor  $D_1(z)$  and the Alcock-Paczynski parameter  $d_L(z)H(z)$  [17]. We will investigate whether different observables are complementary and helpful to reduce the cosmic confusion brought by the spatial curvature and the time-dependent DE EoS.

Let us first go over definitions of different observables. The accelerated expanding universe is described by the Friedmann equation,

$$H^2(z) = H_0^2 [\Omega_m^0 (1+z)^3 + \Omega_D^0 f(z) + \Omega_k^0 (1+z)^2], \quad (3)$$

where  $\Omega_m^0$ ,  $\Omega_D^0$  and  $\Omega_k^0$  refer to densities of matter, dark energy and curvature at the present day in units of the critical density. The function  $f(z)$  is related to the EoS of DE by

$$f(z) = \exp \left[ 3 \int_0^z \frac{1+w(z')}{1+z'} dz' \right]. \quad (4)$$

Besides the Hubble parameter described in Eq. (3), there are other fundamental observables such as the luminosity distance  $d_L(z)$  and the linear growth factor of mass fluctuation  $D_1(z)$ . The luminosity distance  $d_L(z)$  can be expressed as

$$d_L(z) = \frac{1+z}{H_0} \frac{1}{\sqrt{|\Omega_k^0|}} S \left( \sqrt{|\Omega_k^0|} \int_0^z \frac{dz'}{h(z')} \right), \quad (5)$$

where  $h(z) = H(z)/H_0$  and the function  $S(x)$  takes the form  $\sin(x)$ ,  $x$  and  $\sinh(x)$  for a closed, flat and open universe, respectively. The linear growth factor is the solution to the differential equation,

$$\ddot{D}_1 + 2H(z)\dot{D}_1 - \frac{3}{2}\Omega_m H_0^2 (1+z)^3 D_1 = 0 \quad (6)$$

The approximation  $d \log D_1 / d \log a \equiv f(\Omega_m) \approx \Omega_m^{4/7}$  leads the solution of Eq.6 to [4]

$$D_1(z) = \exp \left[ - \int_0^z \frac{dz'}{1+z'} \left( \frac{\Omega_m (1+z')^3}{h(z')} \right)^{4/7} \right]. \quad (7)$$

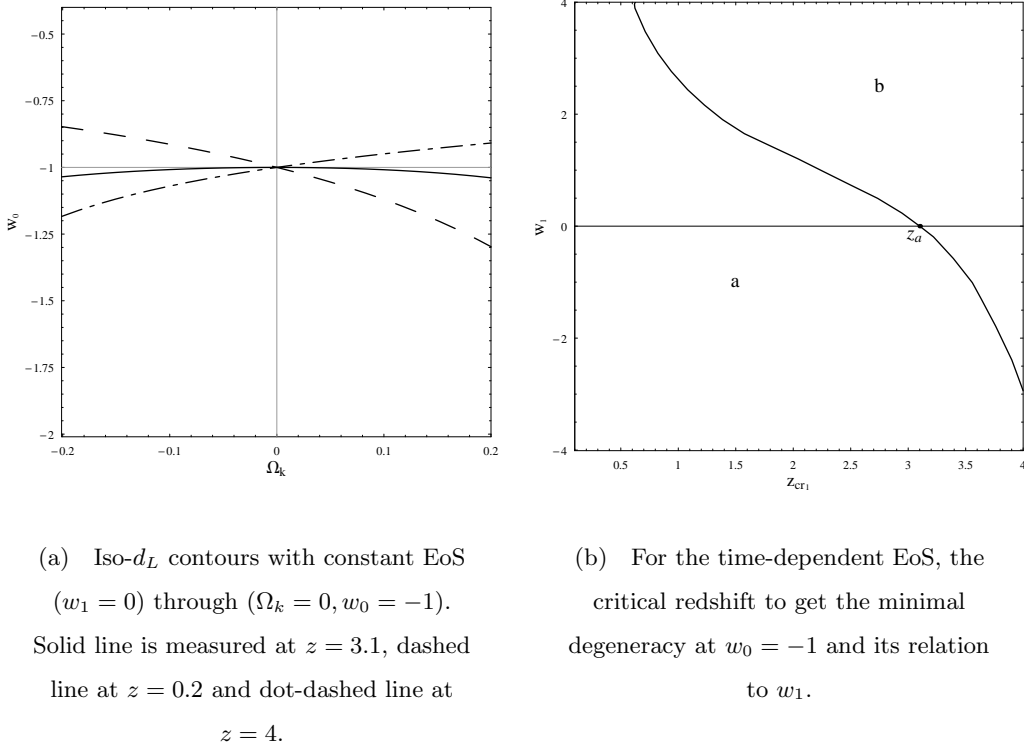
There is another interesting observable called the Alcock-Paczynski (AP) parameter, which is the product  $d_L(z)H(z)$ .

We know that different observations measure different observables. For example, studies of Type IA supernovae measure  $d_L(z)$  directly, while the observations of weak lensing are sensitive to  $D_1(z)$ ,  $d_L(z)$  and  $H(z)$ . The AP parameter is useful in the Alcock-Paczynski anisotropy test [17]. Discussing DE tests in terms of different fundamental observables can show us how different observational strategies complement each other and help to reduce the cosmic confusion.

The cosmic confusion which arises due to a non-vanishing curvature of the universe by considering the luminosity distance  $d_L$  in the two dimensional parameter space  $(\Omega_k^0, w)$  for fixed  $\Omega_m^0$  and arbitrary constant  $w$  has been found in [11]. It was shown that at low redshift  $z_1$ , the iso- $d_L$  curves (having constant  $d_L$  values) display degeneracy in interpreting the observations: a pure cosmological constant  $\Lambda$  assuming a flat universe (Flat- $\Lambda$ ) can equally well be interpreted as Quintessence DE with  $w > -1$  if one takes closed universe (Closed-Q) or Phantom DE with  $w < -1$  if one takes open universe (Open-P) (see dashed line in Fig.1(a)). However at high redshift  $z_2$ , it was found that the degeneracy in the  $(\Omega_k^0, w)$  parameter plane is opposite, the iso- $d_L$  curves display the cosmic confusion among Flat- $\Lambda$ , Closed-P and Open-Q, which is also shown in the dot-dashed line in Fig.1(a). Comparing the property of degeneracies for low and high redshifts, we can constrain the degeneracy in  $w$ . Within the redshift range  $[z_1, z_2]$ , one can find a critical redshift  $z_a$ , which exhibits no degeneracy in  $w$  while maximal degeneracy with respect to the curvature as shown in the solid line in Fig.1(a), when  $\Omega_m^0$  is fixed at 0.3,  $z_a = 3.1$ . At this critical redshift we expect to detect the value of the constant EoS.

It is of great interest to extend the discussion to the time-dependent EoS, since recent analysis indicates that the time varying DE gives a better fit to the type Ia supernova data [18], which mildly favors the evolution of the DE EoS from  $w > -1$  to  $w < -1$  at a recent stage. Theoretical attempts towards understanding the  $w$  crossing  $-1$  phenomenon have been taken [19]. In the following we will use two parameterization models (1) (2) to investigate how a varying EoS would influence the cosmic confusion. We will work now in the three dimensional parameter space  $(\Omega_k^0, w_0, w_1)$  for fixed  $\Omega_m^0$ . We will explain in detail by using the parameterization model (1). The result for the second model (2) is similar.

We consider first the luminosity distance  $d_L$  in our parameter space  $(\Omega_k^0, w_0, w_1)$  measured at fixed redshift  $z$ . For the dynamic EoS, we see that for more positive  $w_1$ , we get much smaller critical redshift  $z_{cr1}$  where we have no degeneracy in  $w_0$  while maximal degeneracy with respect to the curvature. This property is shown in Fig.1(b). At  $w_1 = 0$ ,  $z_{cr1} = z_a = 3.1$ . The region **a** below



Figure

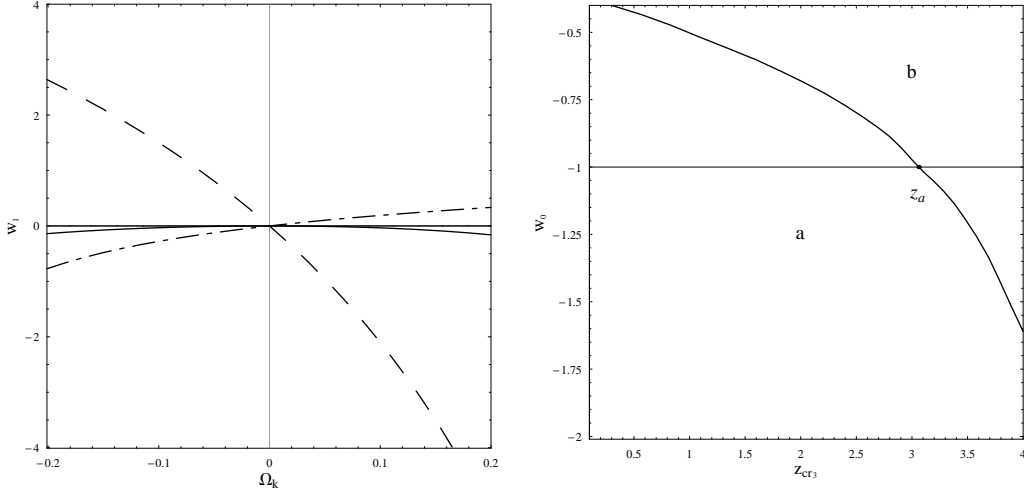
1:

the line in Fig.1(b) contains the cosmic degeneracy in observation (Closed-Q, Flat- $\Lambda$ , Open-P), while the region **b** above has the degeneracy among (Closed-P, Flat- $\Lambda$ , Open-Q).

For fixed  $w_0$ , we have also studied the parameter space  $(\Omega_k^0, w_1)$  in measuring the  $d_L(z)$ . There exists a critical redshift in studying the luminosity distance where there is no degeneracy in  $w_1$  while maximum degeneracy in  $\Omega_k$  which is shown by the solid line in Fig.2(a). This critical redshift which we refer to as  $z_{cr3}$  can help to determine whether  $w_1 = 0$  or not. Fig.2(b) shows that for bigger values of  $w_0$ ,  $z_{cr3}$  could be smaller. At  $w_0 = -1$ ,  $z_{cr3} = z_a = 3.1$ .

Besides the luminosity distance, we have considered other observables, such as the Hubble parameter  $H(z)$ , the linear growth factor  $D_1(z)$  and the AP parameter  $H(z)d_L(z)$ . The Hubble parameter and the linear growth factor have not presented us different degeneracy behavior with the change of the redshift in our parameter space, however the AP parameter gave us the interesting cosmic degeneracy which evolves with the redshift in the interpretation of data. The property of cosmic confusion in our parameter space brought by AP is different from that by  $d_L(z)$ . We will concentrate on the AP parameter in the following.

In our parameter space  $(\Omega_k^0, w_0, w_1)$ , for fixed  $w_1 = 0$ , which is the constant EoS case, the iso-AP curve at low redshift  $z_1$  showed us the cosmic degeneracy in interpreting the observation among



(a) Iso- $d_L$  contours with  $w_0 = -1$  through  $(\Omega_k = 0, w_1 = 0)$ . Solid line is got at  $z = 3.1$ , dashed line at  $z = 0.2$  and dot-dashed line at  $z = 4$ .

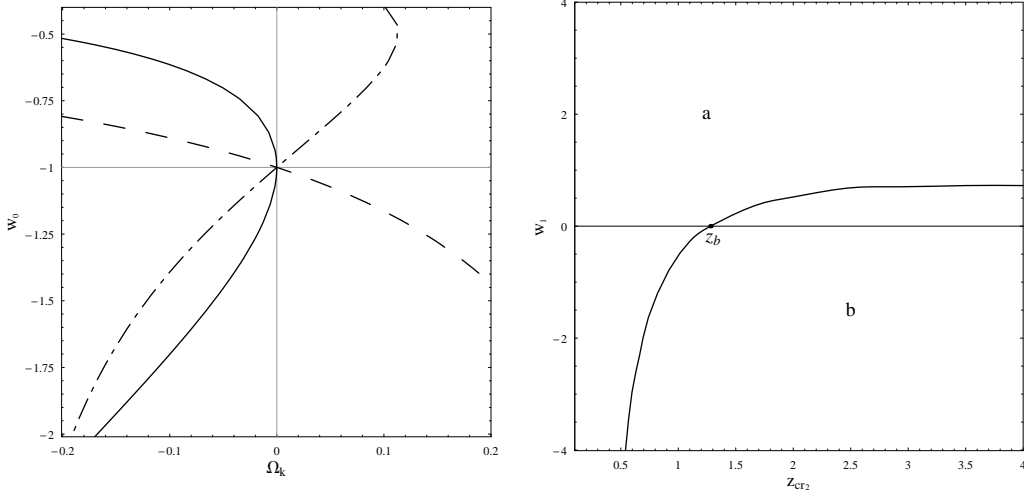
(b) The  $w_0$ -dependence of  $z_{cr3}$ , where minimal degeneracy at  $w_1 = 0$ . When  $w_0 = -1$ ,  $z_a = 3.1$ . Region **a** and region **b** divided by the solid line have different cosmic degeneracy.

Figure

2:

(Closed-Q, Flat- $\Lambda$ , Open-P), while at high redshift  $z_2$  the cosmic confusion arise among (Closed-P, Flat- $\Lambda$ , Open-Q). These are shown in the dashed line and dot-dashed lines in Fig.3(a), respectively. There is a crucial point at the critical redshift between  $z_1$  and  $z_2$ , where the degeneracy behavior changes which is shown by the solid line in Fig.3(a). For  $w_1 = 0$ , this critical redshift is found at  $z_b = 1.3$ , where there is no degeneracy in  $\Omega_k$  while maximum degeneracy in  $w_0$ . This crucial point is interesting since it can help to determine whether  $\Omega_k = 0$  or not.

Now let's extend the discussion to the dynamic DE described in (1). We see from Fig.3(b) that for the more negative  $w_1$  we find smaller critical redshift  $z_{cr2}$  which exhibits minimum degeneracy in  $\Omega_k$  while maximum degeneracy in  $w_0$ , when  $w_1 = 0$ ,  $z_{cr2} = z_b = 1.3$ . Regions above and below the line in Fig.3(b) have different degeneracy in the interpretation of observation: degeneracy among (Closed-Q, Flat- $\Lambda$ , Open-P) in region **a** while degeneracy among (Closed-P, Flat- $\Lambda$ , Open-Q) in region **b**. They represent the cosmic confusion measured at low and high redshifts divided by the critical redshift for fixed  $w_1$ . Drastically different degeneracies straddling the critical redshift can help to determine whether  $\Omega_k = 0$ . However different degeneracies in the parameter space  $(\Omega_k, w_0)$  is not the only criterion to the spatial curvature of the universe. We will further discuss this point in the explanation of Fig.7(b), 8(b) and 9(b).



(a) Iso-AP contours with  $w_1 = 0$  through  $(\Omega_k = 0, w_0 = -1)$ . Solid line is at  $z = 1.3$ , dashed line at  $z = 0.2$  and dot-dashed line at  $z = 4$ .

(b) The critical redshift to get the minimal degeneracy at  $\Omega_k^0 = 0$  and its dependence of  $w_1$ .

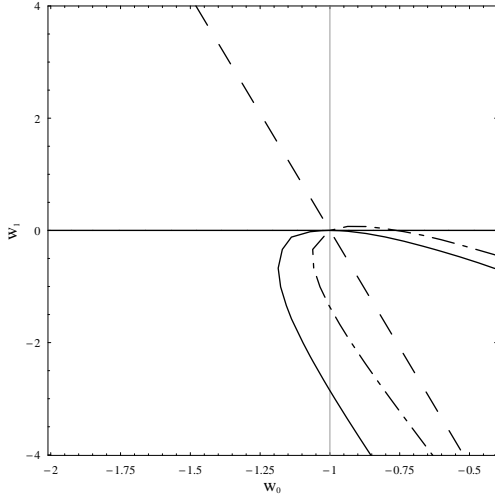
Figure 3:

Fixing  $\Omega_k$ , for example assuming that our universe is flat, from Fig.4(a) we found that there exists a critical redshift  $z_b = 1.3$  where AP parameter essentially presents us no degeneracy in  $w_1$  while maximal degeneracy with  $w_0$  (the solid line). Thus if the spatial curvature of the universe is determined, at this critical redshift AP parameter is useful to conclude whether DE is static or dynamic. For different chosen  $\Omega_k$ , this critical redshift will change as shown in Fig.4(b).

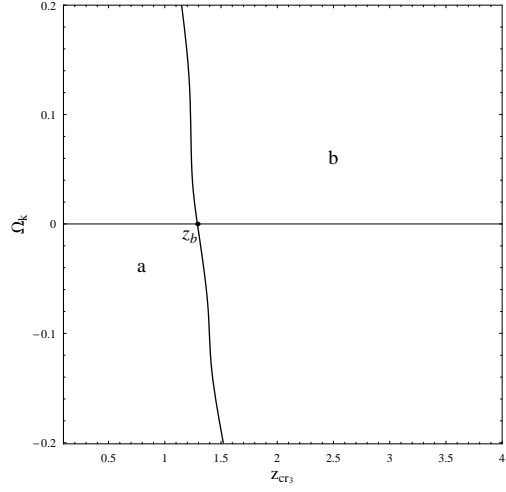
Fig.5(a) shows that for the flat universe, we can also find a critical redshift  $z_c = 2.4$  where from the AP parameter we see no degeneracy in  $w_0$ , while maximum degeneracy in  $w_1$  (the solid line). Fig.5(b) shows that in the universe with some non-zero curvature, this critical redshift will be shifted.

In Fig.6(a), we learnt that for chosen  $w_0 = -1$ , at the redshift  $z_c = 2.4$ , we see no degeneracy in  $\Omega_k$  (solid line). This tells us that if we know  $w_0 = -1$ , the AP parameter observed at  $z_c = 2.4$  can help us to determine whether our universe is flat. Arbitrary values of  $w_1$  will not influence the result. Fig.6(b) exhibits the fact that with the change of chosen  $w_0$  values, the critical value which displays minimum degeneracy in  $\Omega_k$  in the AP parameter will change.

Until now we have discussed the AP parameter measured at different redshifts. In Fig.7(a) we have also exhibited the parameter space  $(\Omega_k^0, w_0)$  with the change of  $w_1$  at the same redshift  $z = 1$ . We observed from the AP parameter measured at the same redshift that with the increase

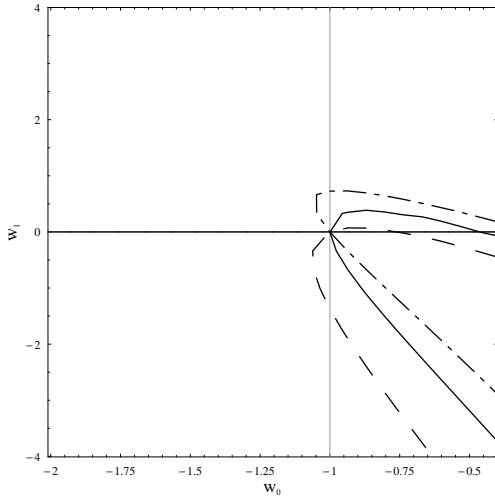


(a) Iso- $AP$  contours with  $\Omega_k = 0$  through  $(w_0 = -1, w_1 = 0)$ . Solid line is at  $z = 1.3$ , dashed line at  $z = 0.2$  and dot-dashed line at  $z = 1.6$ .

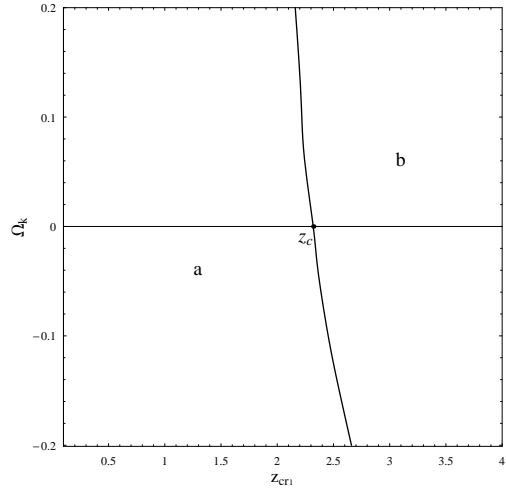


(b) The critical redshift to obtain minimal degeneracy at  $w_1 = 0$  and its relation to  $\Omega_k^0$ .

Figure 4:

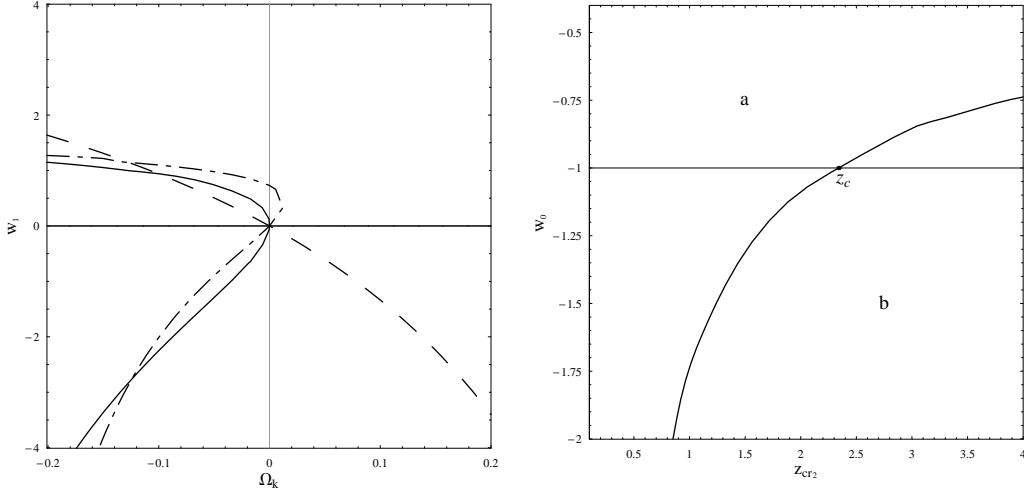


(a) Iso- $AP$  contours with  $\Omega_k = 0$  through  $(w_0 = -1, w_1 = 0)$ . Solid line is at  $z = 2.4$ , dashed line at  $z = 1.6$  and dot-dashed line at  $z = 4$ .



(b) The critical redshift to get the minimal degeneracy at  $w_0 = -1$  and its dependence of the spatial curvature.

Figure 5:



(a) Iso-AP contours with  $w_0 = -1$  through  $(\Omega_k = 0, w_1 = 0)$ . Solid line is for  $z = 2.4$ , dashed line for  $z = 0.2$  and dot-dashed line for  $z = 4$ .

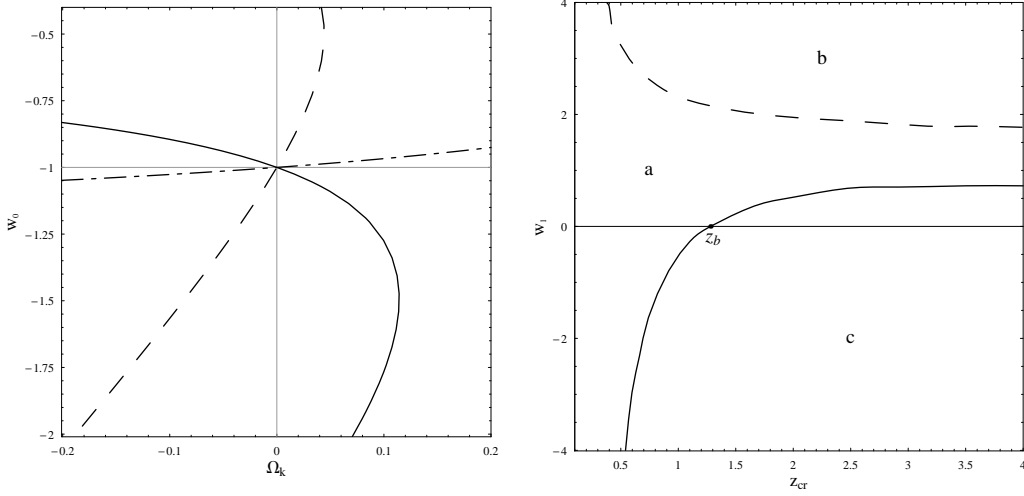
(b) The critical redshift to have minimal degeneracy at  $\Omega_k^0 = 0$  and its dependence of  $w_0$ .

Figure

6:

of  $w_1$  from negative value to the small positive and big positive values, the cosmic confusions vary from the degeneracy of (Closed-P, Flat- $\Lambda$ , Open-Q) (dashed line in Fig.7(a)) to (Closed-Q, Flat- $\Lambda$ , Open-P) (solid line in Fig.7(a)) and back to (Closed-P, Flat- $\Lambda$ , Open-Q) (dot-dashed line in Fig.7(a)). Combining with Fig.3(b), we have plotted Fig.7(b). The solid line in Fig.7(b) can be used to determine whether  $\Omega_k = 0$  for fixed  $w_1$  as discussed in Fig.3(b). Regions **a** and **c** divided by the solid line in Fig.7(b) have different degeneracy behaviors as explained in Fig.3(b). The dashed line in Fig.7(b) is the border separating different cosmic degeneracy behaviors from region **a** (Closed-Q, Flat- $\Lambda$ , Open-P) to region **b** (Closed-P, Flat- $\Lambda$ , Open-Q) observed by the AP parameter with the change of  $w_1$  from small positive value to the big positive value as described in Fig.7(a). From different regions in Fig.7(b), which have opposite degeneracy behaviors with the increase of  $w_1$ , i.e. **a-b** or **a-c**, we can compare these opposite degeneracy at different  $w_1$  for chosen redshifts, for example comparing the solid line with dot-dashed line or solid line with dashed line shown in Fig.7(a), which could help to reduce the uncertainty in the determination whether  $\Omega_k = 0$  through the observations of AP.

Since the recent observation told us that the EoS is in the vicinity of  $w = -1$ , straddling the cosmological constant boundary. In Fig.8, we have examined the cosmic degeneracy by considering AP parameter in the vicinity of  $w_0 = -1$ . In Fig.8(a) we fixed  $\Omega_k = 0$ , and found the degeneracy



(a) Iso-AP contours through  $(\Omega_k = 0, w_0 = -1)$  at redshift  $z = 1$ . Solid line is for  $w_1 = 1$ , dashed line for  $w_1 = -2$  and dot-dashed line for  $w_1 = 3$ .

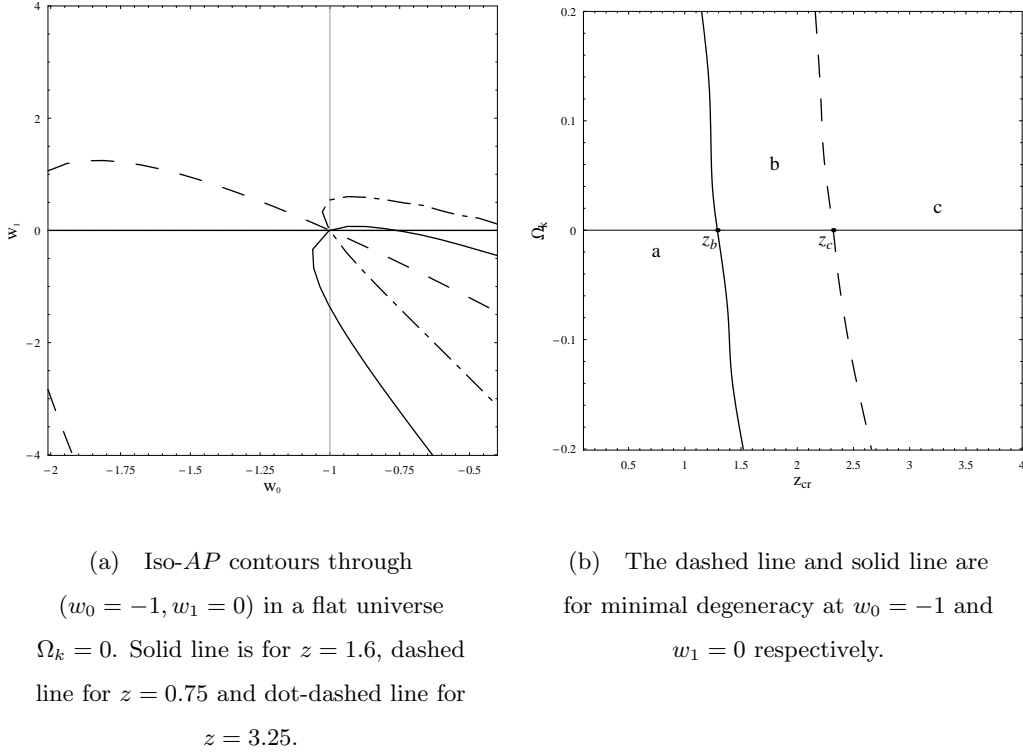
(b) The dashed line and solid line are for minimal degeneracy at  $w_0 = -1$  and  $\Omega_k^0 = 0$ , respectively.

Figure

7:

in parameter space  $(w_0, w_1)$  when interpreting the AP parameter. At low redshift, say  $z = 0.75$ , from the dashed line in Fig.8(a) we obtained the degeneracy between  $(w_0 < -1, w_1 > 0)$  and  $(w_0 > -1, w_1 < 0)$ . The degeneracy behavior changes with the increase of the redshift. When  $z = 1.6$ , the AP parameter presents us the degeneracy between  $(w_0 > -1, w_1 > 0)$  and  $(w_0 < -1, w_1 < 0)$  (see solid line in Fig.8(a)). For  $z = 3.25$ , we have the degeneracy between  $(w_0 > -1, w_1 < 0)$  and  $(w_0 < -1, w_1 > 0)$  (dot-dashed line in Fig.8(a)). For different choices of  $\Omega_k$ , we can also find different degeneracies in  $(w_0, w_1)$  parameter space for the AP parameter. Combining with Fig.4(b) and Fig.5(b), we plotted our Fig.8(b), Different degeneracy behaviors observed at low, intermediate and high redshifts in the parameter space  $(w_0, w_1)$  described in Fig.8(a) are shown in regions **a**, **b**, **c**. They are divided by the solid line and dashed line which can be used to determine whether  $w_1 = 0$  or  $w_0 = -1$  discussed in Fig.4(b) and Fig.5(b), respectively. Similar to Fig.7(b), we can compare observations with testing  $\Omega_k$  and redshift  $z$  in regions **a** and **b** or **b** and **c** in Fig.8(b), which have opposite degeneracies as solid-dashed lines' comparison or solid-dot dashed lines' comparison as illustrated in Fig.8(a), which could constrain  $w_0$  and  $w_1$  around the crucial point  $(w_0 = -1, w_1 = 0)$  in Fig.8(a).

In the above discussion, we have concentrated on the single observable. It is of interest to investigate sensitivities of different observables and see whether they are complementary. Considering the

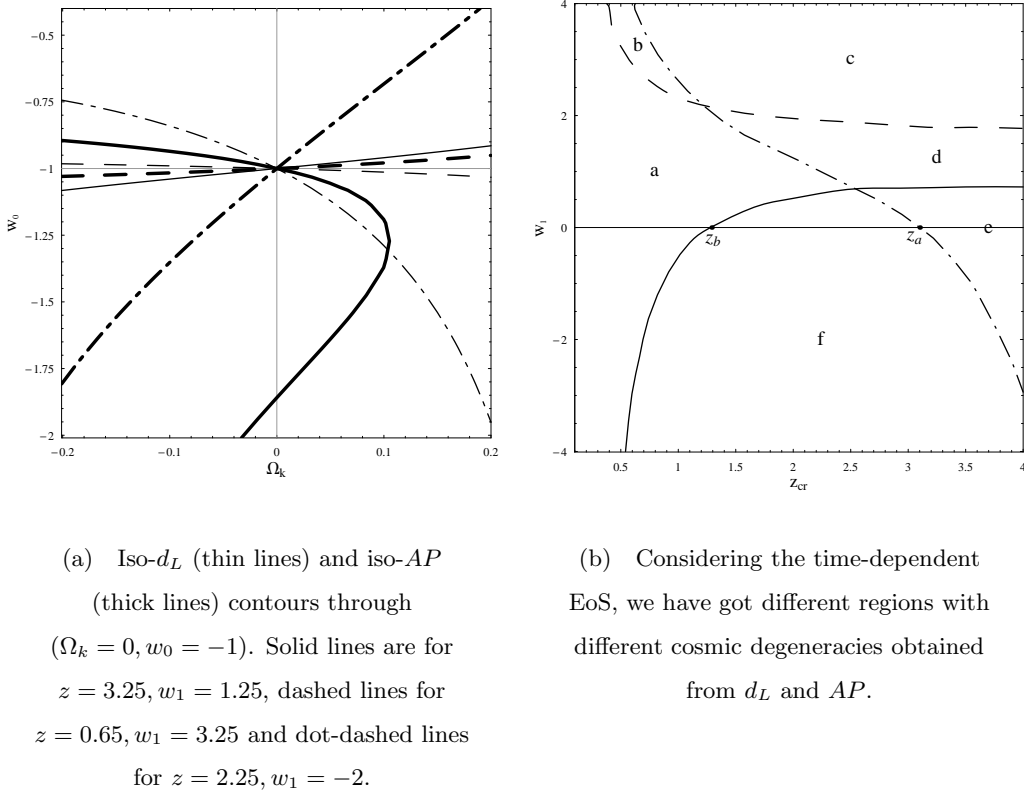


Figure

8:

combination of  $d_L$  and AP, we are going to study how cosmic confusion can arise and be reduced. In Fig.9(a), we have shown the cosmic confusion that arises in the measurements of  $d_L$  and AP with thin and thick lines respectively. For  $z = 3.25$ ,  $w_1 = 1.25$ , from the AP parameter (the thick solid line), we learnt the degeneracy in  $(\Omega_k^0, w_0)$  parameter space among (Closed-Q, Flat- $\Lambda$ , Open-P) while the degeneracy obtained from the  $d_L$  is (Closed-P, Flat- $\Lambda$ , Open-Q) (see thin solid line). For  $z = 2.25$ ,  $w_1 = -2$ , the AP parameter measurement presents us the cosmic confusion among (Closed-P, Flat- $\Lambda$ , Open-Q) (the thick dot-dashed line), however the  $d_L$  observation gives the confusion among (Closed-Q, Flat- $\Lambda$ , Open-P) (thin dot-dashed line). For  $z = 0.65$ ,  $w_1 = 3.25$ , the interpretations of the AP parameter and  $d_L$  also display different confusion behaviors as (Closed-P, Flat- $\Lambda$ , Open-Q) from AP (thick dashed line) and (Closed-Q, Flat- $\Lambda$ , Open-P) from  $d_L$  (thin dashed line). Different cosmic degeneracy behaviors from different observables are possible to be used to reduce the confusion. In Fig.9(b), we have combined the Fig.9(a) with properties exhibited in Fig.7(b) learnt from the AP parameter and Fig.1(b) obtained from  $d_L$ . From Fig.7(b), we learnt that region **a** and **f** shown in Fig.9(b) have different degeneracy behaviors interpreted from the AP parameter: **a**:(Closed-Q, Flat- $\Lambda$ , Open-P) and **f**: (Closed-P, Flat- $\Lambda$ , Open-Q). As exhibited in Fig.9(a) for  $z = 3.25$ ,  $w_1 = -2$ , if we consider the luminosity distance, we obtain opposite

degeneracy in region **f**. Different cosmic confusions in regions **a** and **d** have also been found in Fig.1(b) in the interpretation of  $d_L$  and we know **a**: (Closed-Q, Flat- $\Lambda$ , Open-P) and **d**: (Closed-P, Flat- $\Lambda$ , Open-Q). If we examine the cosmic degeneracy in region **d** from the AP, it is different from that learnt from the observable  $d_L$ , which was explained in Fig.9(a) for  $z = 3.25, w_1 = 1.25$ . The region **b** persists the degeneracy behaviors shown in Fig.9(a) at  $z = 0.65, w_1 = 3.25$ , which are opposite for observables AP and  $d_L$ . Again, we can take advantage of the opposite degeneracies with  $w_1$ 's and redshift  $z$ 's in region **b**, **d** or **f** to reduce the cosmic confusion. The point that different regions shown in Fig.9(b) have different cosmic confusions by considering the luminosity distance and the AP parameter is interesting since this property shows that these two observables are complementary and it could be helpful to reduce the uncertainty in observation interpretation.



Figure

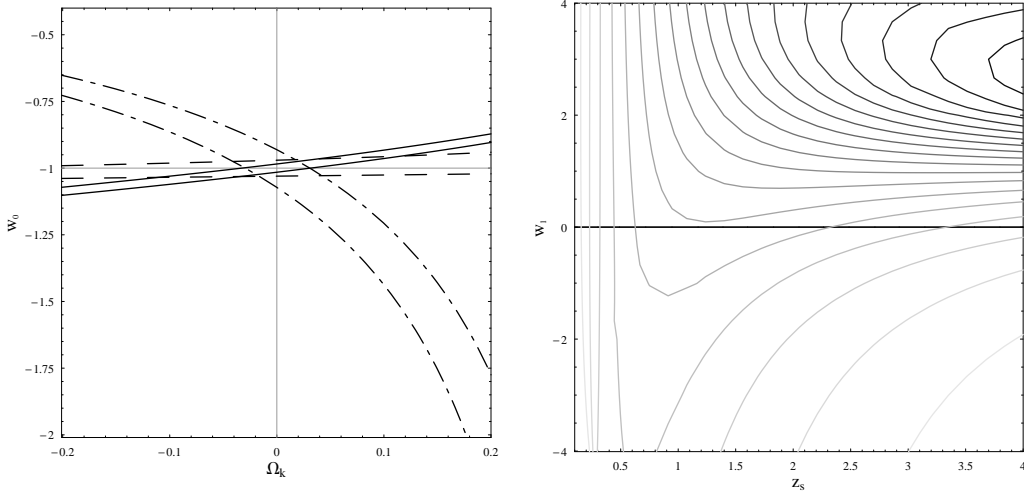
9:

To reduce the cosmic confusion, another important factor we need to take into account is the error sensitivity of observables. If we consider the relative error of an observable, for instance  $\frac{\delta d_L}{d_L} \sim 1\%$  for the luminosity distance, the single curve of each observable will be replaced by a band. Such a band certainly covers more than a single curve in the parameter space and will complicate the degeneracy analysis above. The width of the band is relevant to the redshift. At

different redshift, the same amount of error has different width in the parameter space, which represents the error sensitivity of the observable. The narrower the band is, the more sensitive the observable is to the error. Mathematically the error sensitivity of  $d_L$  can be quantitatively defined as derivatives of  $d_L$  with respect to  $\Omega_k$  and  $w_0$  at  $\Omega_k = 0$ ,  $w_0 = -1$ ,

$$\xi_{d_L}(z, w_1) = \frac{\partial^2 d_L(z, \Omega_k, w_0, w_1)}{\partial \Omega_k \partial w_0} \Big|_{\Omega_k=0, w_0=-1}, \quad (8)$$

and the large value of the  $\xi$  corresponds to high sensitivity. The values of  $\xi_{d_L}(z, w_1)$  result in the choices in the parameter space  $(z, w_1)$ . As shown in Fig.10(b), sensitivity decreases with the brightness of contour lines, thus the error sensitivity is high at high  $z$  for  $w_1 > 0$ . In Fig.10(a), sample plot shows that with the same relative error, the higher the sensitivity, the narrower the error band in  $(\Omega_k^0, w_0)$  parameter space for  $d_L$ .



(a) Iso- $d_L$  contours with 1% error around  $(\Omega_k = 0, w_0 = -1)$ . Solid lines are for  $z = 4, w_1 = 3$ , dashed lines for  $z = 1.5, w_1 = 2$  and dot-dashed lines for  $z = 1, w_1 = -2$ .

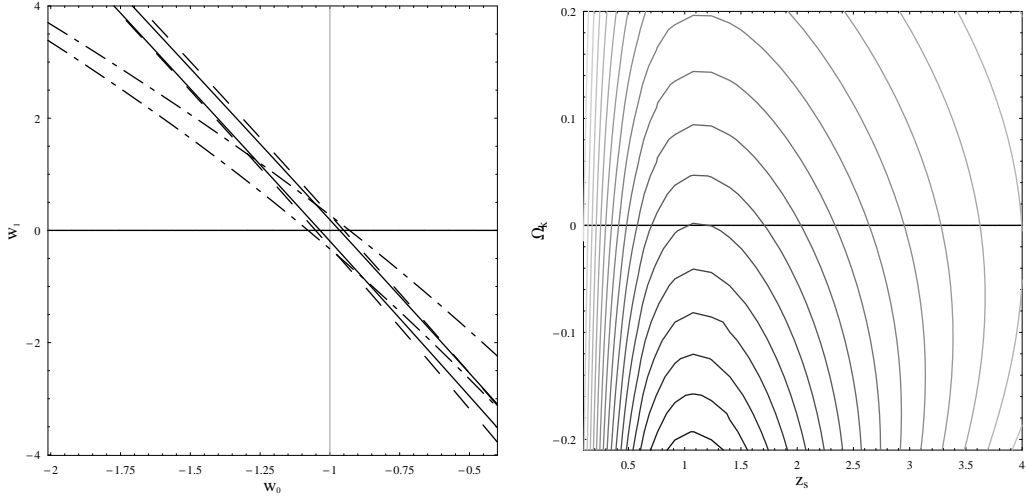
(b) Error sensitivity dependence of  $w_1$  and the redshift.

Figure

10:

Fig.11 shows that for the same relative error, the band in the parameter space  $(w_0, w_1)$  for  $d_L$  is narrower with positive curvature and small redshift. Similarly Fig.12 displays the narrower band in the parameter space  $(\Omega_k, w_1)$  for  $d_L$  at high  $z$  and  $w_0 > -1$ .

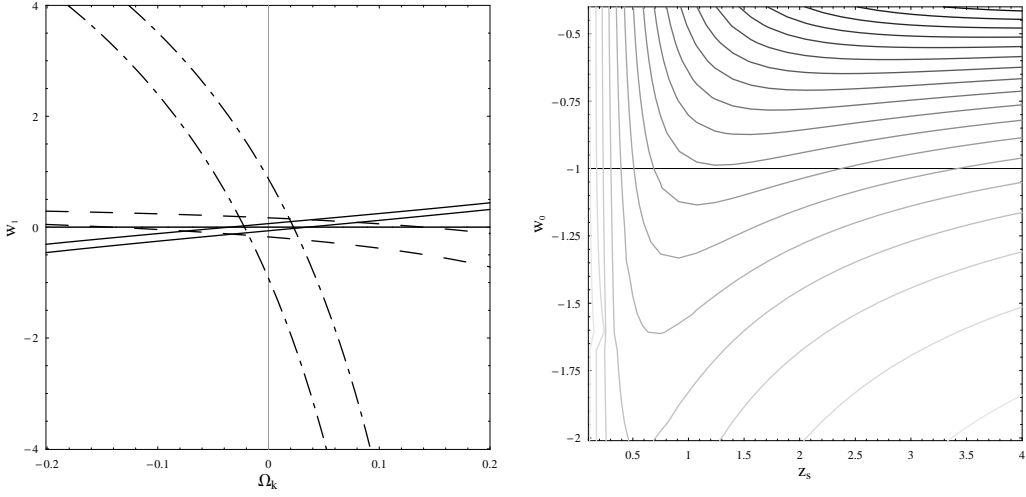
Studying the width of band for the same relative error of the observable AP parameter, we obtained the possibility of obtaining the tighter bound in the parameter spaces  $(\Omega_k, w_0)$  (Fig.13)



(a) Iso- $d_L$  contours with 1% error around  $(w_0 = -1, w_1 = 0)$ . Solid lines are for  $z = 1, \Omega_k = -0.2$ , dashed lines for  $z = 1, \Omega_k = 0$  and dot-dashed lines for  $z = 3, \Omega_k = 0.15$ .

(b) Error sensitivity dependence of  $\Omega_k^0$  and the redshift.

Figure 11:

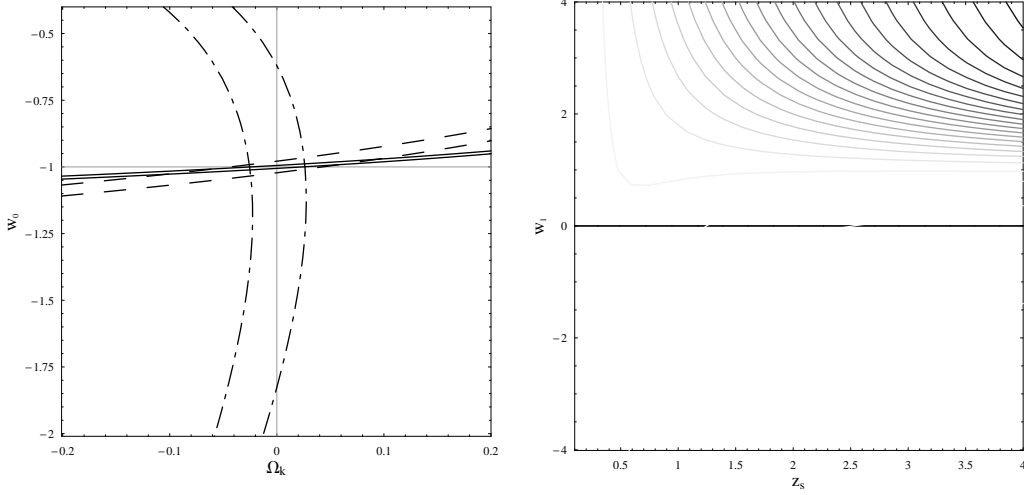


(a) Iso- $d_L$  contours with 1% error around  $(\Omega_k = 0, w_1 = 0)$ . Solid lines are for  $z = 4, w_0 = -0.4$ , dashed lines for  $z = 1.5, w_0 = -0.75$  and dot-dashed lines for  $z = 0.5, w_0 = -2$ .

(b) Error sensitivity dependence of  $w_0$  and the redshift.

Figure 12:

and  $(w_0, w_1)$  (Fig.14) for the same requirements as that of the observable  $d_L$ . In the parameter space  $(\Omega_k, w_1)$ , the narrower band of AP for the same relative error can be got at low redshift and  $-1 < w_0 < -1/3$  (Fig.15), which is not exactly the same as that of the luminosity distance.



(a) Iso- $AP$  contours with 1% error around  $(\Omega_k = 0, w_0 = -1)$ . Solid lines are for  $z = 4, w_1 = 4$ , dashed lines for  $z = 1, w_1 = 4$  and dot-dashed lines for  $z = 0.5, w_1 = -4$ .

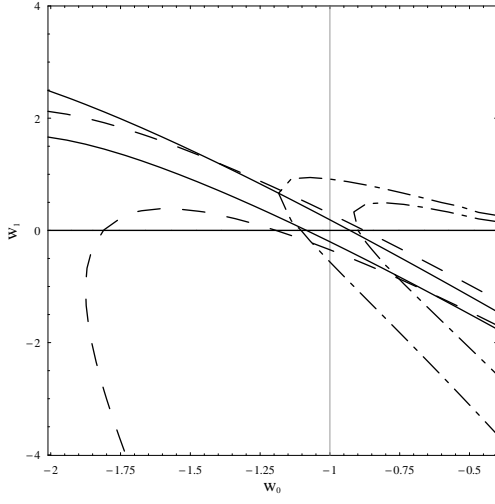
(b) Error sensitivity dependence of  $w_1$  and the redshift.

Figure

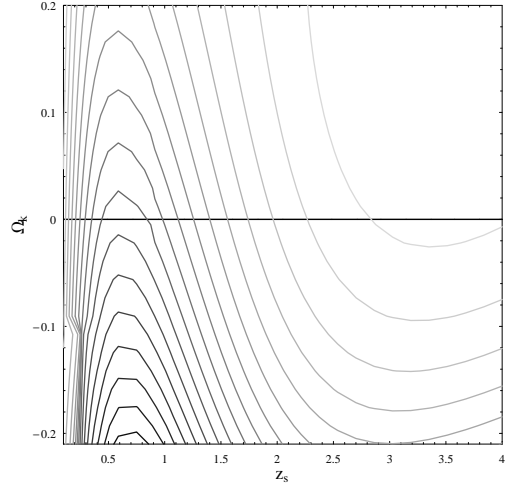
13:

For the same relative error, a narrower band of an observable is more interesting, since it can put more stringent constraints on the parameter space, which can be more useful to reduce the cosmic confusion if we employ the properties we learnt in Fig.1-9.

In summary, we have extended the discussion of the uncertainty on the determination of the DE of constant EoS due to a non-vanishing spatial curvature by considering the luminosity distance [11] to the dynamic DE models by considering other fundamental observables. We discussed the sensitivity of these observables to the value and redshift history of the EoS and the spatial curvature, investigated whether these different observables are complementary. Since the observables we studied in this paper are measured nearly in all proposed tests of DE, we expect that our analysis can be useful in the future observations in determining the nature of the DE.

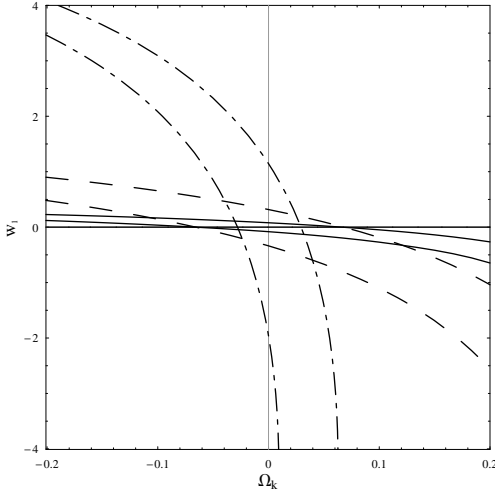


(a) Iso- $AP$  contours with 1% error around  $(w_0 = -1, w_1 = 0)$ . Solid lines are for  $z = 0.75, \Omega_k = -0.2$ , dashed lines for  $z = 0.75, \Omega_k = 0$  and dot-dashed lines for  $z = 3.5, \Omega_k = 0.1$ .

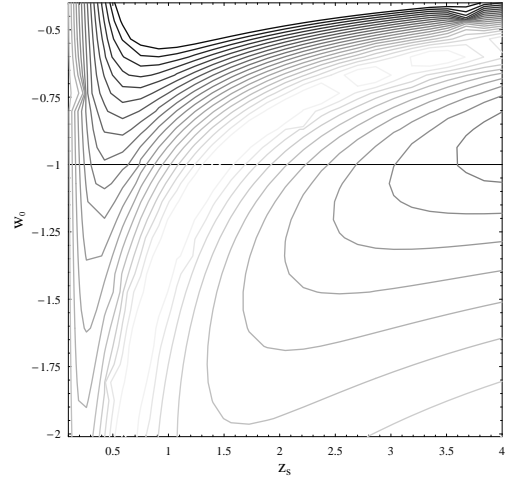


(b) Error sensitivity dependence on  $\Omega_k^0$  and the redshift.

Figure 14:



(a) Iso- $AP$  contours with 1% error around  $(\Omega_k = 0, w_1 = 0)$ . Solid lines are for  $z = 1.5, w_0 = -0.4$ , dashed lines for  $z = 0.5, w_0 = -0.8$  and dot-dashed lines for  $z = 0.5, w_0 = -2$ .



(b) Error sensitivity depending on  $w_0$  and the redshift.

Figure 15:

## Acknowledgments

This work was partially supported by NNSF of China, Ministry of Education of China and Shanghai Education Commission. B. Wang would like to acknowledge helpful discussions with E. Abdalla and R. G. Cai.

- 
- [1] A. G. Riess et al, *Astron. J.* **116** (1998) 1009; S. Perlmutter et al, *Astrophys. J.* **517** (1999) 565; S. Perlmutter et al, *Astrophys. J.* **598** (2003) 102; P. de Bernardis et al, *Nature* **404** (2000) 955.
  - [2] T. Padmanabhan, *Phys. Rept.* **380**, 235 (2003), hep-th/0212290; P. J. E. Peebles, B. Ratra, *Rev. Mod. Phys.* **75**, 559 (2003), astro-ph/0207347; V. Sahni, astro-ph/0403324 and references therein.
  - [3] R. Caldwell, M. Doran, *Phys. Rev. D* **69** (2004), 103517.
  - [4] Hogg, D.W. 1999, astro-ph/9905116
  - [5] D. H. Weinberg, *New Astron. Rev.* **49** (2005) 337-345
  - [6] J. L. Sievers et al., *Astrophys. J.* **591** (2003) 599; C. B. Netterfield et al., *Astrophys. J.* **571**, 604 (2002); A. Benoit et al., *Astron. Astrophys.* **399** (2003) L25; ibid 399 (2003) L19.
  - [7] J. P. Uzan, U. Kirchner and G. F. R. Ellis, *Mon. Not. Roy. Astron. Soc.* **344** (2003) L65; A. Linde, *JCAP* **0305** (2003) 002; M. Tegmark, A. de Oliveira-Costa and A. Hamilton, *Phys. Rev. D* **68** (2003) 123523; G. Efstathiou, *Mon. Not. Roy. Astron. Soc.* **343** (2003) L95; J. P. Luminet, J. Weeks, A. Riazuelo, R. Lehou and J. Uzan, *Nature* **425** (2003) 593; G. F. R. Ellis and R. Maartens, *Class. Quant. Grav.* **21** (2004) 223.
  - [8] R. R. Caldwell and M. Kamionkowski, astro-ph/0403003; B. Wang, Y. G. Gong and R. K. Su, hep-th/0408032, *Phys. Lett. B* **605** (2005) 9.
  - [9] E. V. Linder, *Astropart. Phys.* **24** (2005) 391-399
  - [10] E. V. Linder, *Testing Consistency of  $\Omega_\Lambda - \Omega_M$  Plots and Flatness*, <http://supernova.lbl.gov/~evlinder/noflat.pdf> (2002)
  - [11] D. Polarski, A. Ranquet, *Phys. Lett. B* **627** (2005) 1-8
  - [12] H. K. Jassal, J. S. Bagla and T. Padmanabhan, *Mon. Not. Roy. Astron. Soc.* **356** (2005) L11-L16.
  - [13] M. Chevallier and D. Polarski, *Int. J. Mod. Phys. D* **10** (2001) 213; E. V. Linder, *Phys. Rev. Lett.* **90**, (2003) 91301; E. V. Linder, *Phys. Rev. D* **70** (2004) 023511.
  - [14] T. R. Choudhury and T. Padmanabhan, *Astron. Astrophys.* **429** (2005) 807.
  - [15] Y. G. Gong, *Class. Quant. Grav.* **22** (2005) 2121-2133.
  - [16] A. G. Riess et. al., *Astrophys. J.* **607** (2004) 665-687; U. Alam, V. Sahni, T. D. Saini and A. A. Starobinsky, *Mon. Not. Roy. Astron. Soc.* **354** (2004) 275; U. Alam, V. Sahni and A. A. Starobinsky, *JCAP* **0406** (2004) 008.
  - [17] Alcock, C., & Paczyński, B. 1979, *Nature*, 281, 358

- [18] U. Alam, V. Sahni, A. A. Starobinsky, *JCAP* **0406** (2004) 008; D. Huterer, A. Cooray, *Phys. Rev.* **D71** (2005) 023506; Y. Wang, M. Tegmark, astro-ph/0501351; H.K.Jassal, J.S.Bagla, T. Padmanabhan astro-ph/0506748.
- [19] B. Wang, Y. G. Gong and E. Abdalla, *Phys. Lett.* **B624** (2005) 141; B. Wang, C. Y. Lin and E. Abdalla, *Phys. Lett.* **B624** (in press); S. Nojiri and S. D. Odintsov, *Phys. Rev.* **D70** (2004) 103522 hep-th/0408170; S. Nojiri, S.D. Odintsov and S. Tsujikawa, *Phys. Rev.* **D71** (2005) 063004 hep-th/0501025; B. Feng, X. L.Wang and X. M. Zhang, *Phys. Lett.* **B 607**, 35 (2005); W. Hu, *Phys. Rev.* **D 71**, 047301 (2005) [arXiv:astro-ph/0410680]; Z. K. Guo, Y. S. Piao, X. M. Zhang and Y. Z. Zhang, *Phys. Lett.* **B 608**, 177 (2005); X.F. Zhang, H.Li, Y.S. Piao and X. Zhang, astro-ph/0501652; M. Z. Li, B. Feng and X. M. Zhang, arXiv:hep-ph/0503268; R. G. Cai, H. S. Zhang and A. Z. Wang, hep-th/0505186; H. Stefancic, astro-ph/0504518.